

Article

Remarkable Increase of Fluorescence Quantum Efficiency by Cyano Substitution on an ESIPT Molecule 2-(2-Hydroxyphenyl)benzothiazole: A Highly Photoluminescent Liquid Crystal Dopant

Tsuneaki Sakurai ^{1,*} , Masaya Kobayashi ¹, Hiroyuki Yoshida ² and Masaki Shimizu ¹

¹ Faculty of Molecular Chemistry and Engineering, Kyoto Institute of Technology, Hashikami-cho, Matsugasaki, Sakyo-ku, Kyoto 606-8585, Japan; b8151062@edu.kit.ac.jp (M.K.); mshimizu@kit.ac.jp (M.S.)

² Division of Electrical, Electronic and Infocommunications Engineering, Osaka University, 2-1 Yamadaoka, Suita 565-0871, Japan; yoshida@eei.eng.osaka-u.ac.jp

* Correspondence: sakurai@kit.ac.jp

Abstract: Fluorescent molecules with excited-state intramolecular proton transfer (ESIPT) character allow the efficient solid-state luminescence with large Stokes shift that is important for various applications, such as organic electronics, photonics, and bio-imaging fields. However, the lower fluorescence quantum yields (Φ_{FL}) in the solution or viscous media, due to their structural relaxations in the excited state to reach the S_0/S_1 conical intersection, shackle further applications of ESIPT-active luminophores. Here we report that the introduction of a cyano group (-CN) into the phenyl group of 2-(2-hydroxyphenyl)benzothiazole (**HBT**), a representative ESIPT compound, remarkably increase its fluorescence quantum yield (Φ_{FL}) from 0.01 (without -CN) to 0.49 (with -CN) in CH_2Cl_2 , without disturbing its high Φ_{FL} (=0.52) in the solid state. The large increase of the solution-state Φ_{FL} of the cyano-substituted HBT (**CN-HBT**) is remarkable, comparing with our previously reported Φ_{FL} values of 0.05 (with 4-pentylphenyl), 0.07 (with 1-hexynyl), and 0.15 (with 4-pentylphenylethynyl). Of interest, the newly-synthesized compound, **CN-HBT**, is miscible in a conventional room-temperature nematic liquid crystal (LC), 4-pentyl-4'-cyano biphenyl (5CB), up to 1 wt% (~1 mol%), and exhibits a large Φ_{FL} of 0.57 in the viscous LC medium. A similar Φ_{FL} value of $\Phi_{FL} = 0.53$ was also recorded in another room-temperature LC, *trans*-4-(4-pentylcyclohexyl)benzonitrile (PCH5), with a doping ratio of 0.5 wt% (~0.5 mol%). These 5CB/**CN-HBT** and PCH5/**CN-HBT** mixtures serve as light-emitting room-temperature LCs, and show anisotropic fluorescence with the dichroic ratio of 3.1 upon polarized excitation, as well as electric field response of luminescence intensity changes.

Keywords: cyano group; ESIPT; fluorescence; host-guest liquid crystal; luminescent liquid crystal



Citation: Sakurai, T.; Kobayashi, M.; Yoshida, H.; Shimizu, M. Remarkable Increase of Fluorescence Quantum Efficiency by Cyano Substitution on an ESIPT Molecule 2-(2-Hydroxyphenyl)benzothiazole: A Highly Photoluminescent Liquid Crystal Dopant. *Crystals* **2021**, *11*, 1105. <https://doi.org/10.3390/cryst11091105>

Academic Editor: Ana M. Garcia-Deibe

Received: 19 August 2021

Accepted: 8 September 2021

Published: 10 September 2021

Publisher's Note: MDPI stays neutral with regard to jurisdictional claims in published maps and institutional affiliations.



Copyright: © 2021 by the authors. Licensee MDPI, Basel, Switzerland. This article is an open access article distributed under the terms and conditions of the Creative Commons Attribution (CC BY) license (<https://creativecommons.org/licenses/by/4.0/>).

1. Introduction

The light-emitting nematic liquid crystal (LC) phase at room temperature is important for polarizer-less display applications with bright and low-power characteristics [1–4]. Nevertheless, it is quite challenging, by using a single new compound, to obtain nematic LC phases with a single molecule in a wide temperature range covering room temperature. The mixing strategy, a characteristic feature of LC materials, is a solution to overcome this challenge, which is utilized for the preparation of functional room-temperature LCs—functional molecules are doped in a known room-temperature LCs. These doping systems are also called as host-guest LCs, where functional molecules (=dopant) are “guest” and room temperature LCs are “host”. Dye-doped LCs were proposed earlier as such host-guest LCs, for the application of new display systems [5–7]. They have been considered available for other applications, such as optical storage devices [8], security devices [9], and smart windows [10]. Light-emitting nematic LCs are accessible by such host-guest LCs using a luminescent dopant and room-temperature LC. Miscibility in the host LCs and efficient emission are the basic requisites for the luminescent dopant molecules. Visible-region luminescent molecules composed of rod-shaped, small-size aromatic cores are

promising for sufficient miscibility. In this context, our group has focused on the use of excited-state intramolecular proton transfer (ESIPT)-type fluorescent dopants based on 2-(2-hydroxyphenyl)benzothiazole (HBT) [11–14]. The HBT-based molecules have relatively small aromatic cores compared with typical dye molecules. Moreover, they have a benefit of transparency in the visible region, but they are photoluminescent in green color (~530 nm) upon ultraviolet excitations, which rely on the large Stokes shift due to the four-level photo cycle including the ESIPT between *enol* and *keto* tautomers (Figure 1) [15–18].

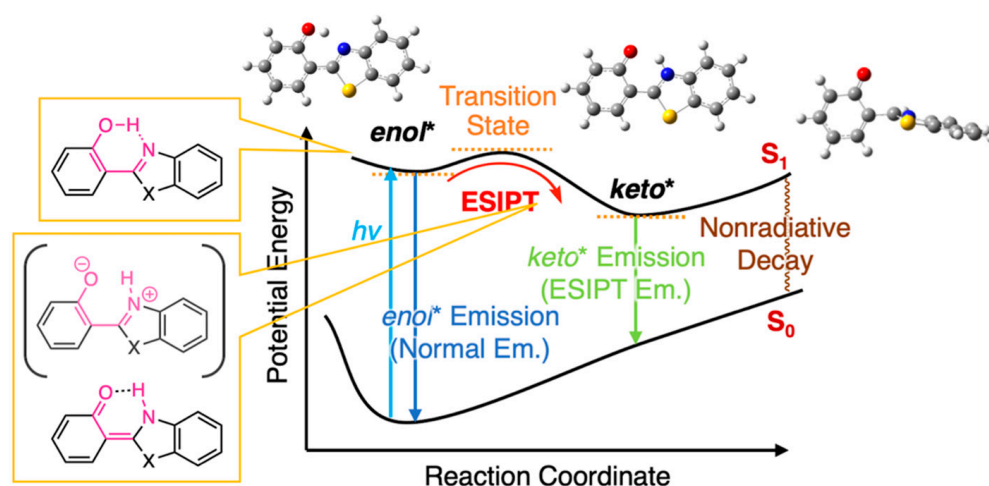


Figure 1. Schematic illustration of potential energy diagram of ESIPT process in 2-(2-hydroxyphenyl)benzazole.

Previously, we discussed that ESIPT molecules inherently possess the aggregation-induced emission (AIE) character [19,20] and tend to be less or almost non emissive in a solution state due to the structural relaxation in the excited state to approach conical intersections from the *keto** state by a bond rotation (Figure 1), resulting in the acceleration of nonradiative decays [11,12,14]. However, we discovered that the introduction of aryl [11], alkynyl [12] or arylene ethynylene [14] groups into HBT (Figures 2 and S1) increases the fluorescence quantum yield (Φ_{FL}) up to 0.15 in CH_2Cl_2 [14] ($\Phi_{FL} = 0.01$ for HBT in CH_2Cl_2 ; Figure 2). Of interest, room-temperature LC hosts, such as 4-cyano-4'-pentylbiphenyl (5CB), can be treated as viscous solvents—the absolute values of Φ_{FL} in 5CB are larger than those in CH_2Cl_2 , which can be explained by assuming that the rotation of the carbon–carbon bond between 2-hydroxyphenyl and benzothiazole units is dependent on the viscosity of the surrounding media [21,22]. The largest value of Φ_{FL} in 5CB is 0.32 among those of the HBT derivatives we developed thus far [12,14]. Meanwhile, Jacquemin, Massue, Ulrich and coworkers have reported the positive effect of silylethynyl groups introduced in 2-(2-hydroxyphenyl)benzoxazole (HBO) on the value of Φ_{FL} in organic solvents [23–26] and recently extended the findings to HBT and 2-(2-hydroxyphenyl)benzimidazole (HBI) [27]. They and we have independently mentioned the impact of the introduced alkyne groups on the restriction of rotation around the C–C bonds in HBT or HBO [12,14,26,27]. Zhang and coworkers have also reported arylethynyl-extended HBT derivatives [28,29]. Although these studies indicate the importance of alkyne substituents for the HBT, HBO and HBI series, the molecular design of the ESIPT compounds still needs to be improved for maximizing the potential of efficient ESIPT fluorescence in solvents and host LCs.

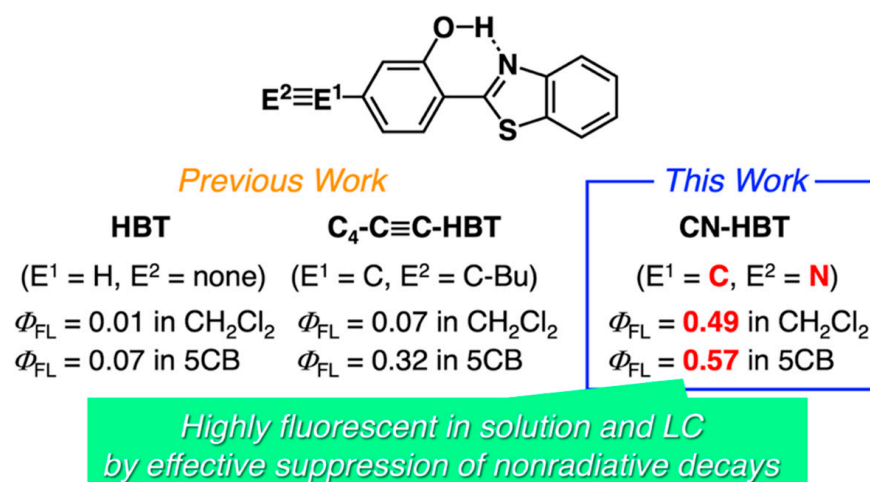


Figure 2. Molecular design of highly fluorescent HBT derivatives.

In this article, we report that the introduction of a cyano group into the 4-position of 2-hydroxyphenyl group in HBT drastically increase its Φ_{FL} from 0.01 (**HBT**) to 0.49 (with -CN) in CH₂Cl₂, without disturbing its high Φ_{FL} (=0.52) in the solid state (Figure 2). The large increase of the solution-state Φ_{FL} of the cyano-substituted HBT (**CN-HBT**) is remarkable, comparing with our previously reported Φ_{FL} values of 0.05 (with 4-pentylphenyl; **C₅P-HBT**), 0.07 (with 1-hexynyl, **C₄-C≡C-HBT**), and 0.15 (with 4-pentylphenylethynyl, **C₅P-C≡C-HBT**) (Figure 2). It should be noted that **CN-HBT** is recently reported as an example of the products in the development of photoredox-type C–H hydroxylation reactions [30,31], but no study on the photophysical properties was reported except for one article that focused on the use of HBT derivatives including **CN-HBT** as a γ -ray radiation scintillator [32]. Polystyrene films doped with **CN-HBT** were exposed to irradiation and the generated excited states emit *keto** emission. However, no detailed studies by UV light excitations nor quantitative discussions were reported. Here we found that **CN-HBT** is miscible in 5CB up to 1 wt% (~1 mol%), and exhibits a large Φ_{FL} of 0.57. Further detailed experiments confirm the anisotropic absorption and fluorescence of **CN-HBT** in 5CB, revealing its potential as a new ESIPT-based LC dopant with highly efficient fluorescence.

2. Materials and Methods

2.1. General Methods

All the chemicals were purchased from Tokyo Chemical Industry Co. Ltd. (Tokyo, Japan), Fujifilm Wako Pure Chemical Co. (Osaka, Japan), or Merck and Co. (Sigma-Aldrich) (St. Louis, MO, USA), and used as received. TLC analyses were performed on a glass coated with Silica gel 70 F₂₅₄ purchased from Fujifilm Wako Pure Chemical Co. Column chromatography was performed on PSQ60B silica gel (spherical) purchased from Fuji Silysia Chemical Ltd. (Aichi, Japan). ¹H-NMR and ¹³C-NMR spectra were recorded in CDCl₃ on a Varian Mercury 400 spectrometer, operating at 400 and 100 MHz, respectively, where chemical shifts were determined with respect to tetramethylsilane (TMS, δ 0.00) or CHCl₃ as an internal reference. All the mixtures of 5CB/**CN-HBT** and PCH5/**CN-HBT** were prepared in the glass vial at corresponding weight ratios. Each mixture was heated to 50 °C to give transparent homogenous mixtures and allowed to cool down to room temperature.

2.2. Phase Characterizations

The optical textures were recorded by an Olympus BX53-P polarizing optical microscope (POM) equipped with a Mettler HS82 hot-stage system, where the sample was loaded into a 5- μ m thick sandwiched glass cell without surface treatment. Phase transition behaviors were characterized by a Hitachi High-Tech Science Corporation DSC620

differential scanning calorimeter (DSC). The 1st heating run was started from 30 °C at 10 K min⁻¹, and further heat/cool cycles were conducted at the same scan rate. X-ray diffraction (XRD) experiments of the powders of the **CN-HBT** and 5CB/**CN-HBT** mixtures were carried out using a Rigaku MiniFlex600 X-ray diffractometer ($\lambda = 1.54 \text{ \AA}$) with a D/teX Ultra semiconductor detector. The sample was mounted on a silicon non-reflecting plate.

2.3. Absorption and Fluorescence Spectroscopy

Electronic absorption spectra were recorded on a JASCO V-750 spectrometer. Polarizing absorption spectra were carried out using a WP25M-UB mounted wire grid polarizer ($\varphi \sim 25 \text{ mm}$). Fluorescence spectra were measured on a JASCO FP-8500 fluorescence spectrophotometer. Absolute fluorescence quantum yields (Φ_{FL}) were evaluated on this spectrometer with a JASCO ILF-835 fluorescence integrate sphere unit.

2.4. Fluorescence Lifetime Measurements

Fluorescence lifetimes were evaluated on a Hamamatsu Photonics Quantaaurus- τ using 365 nm LED excitation pulses. Fluorescence decay profiles were obtained by averaging a 20 nm range around the peak wavelength. The measurements were performed using powders of **CN-HBT** and 5CB/**CN-HBT** (99/1 wt/wt) LCs in a quartz petri dish, and a CH₂Cl₂ solution of **CN-HBT** (50 μM) in a 1 \times 1 cm quartz cell.

2.5. Polarizing Fluorescence Microscopy

Fluorescence anisotropy was evaluated by micro-spectroscopy of polarized fluorescence. Glass sandwich cells with a cell-gap of 15 μm and a parallel rubbing treatment on both substrates were purchased from EHC Co., Japan. A 5CB/**CN-HBT** mixture was injected in the cell by capillary action and observed under a Nikon Eclipse LV100N-POL POM with fluorescence measurement capability using a $\times 10$ objective lens. UV light ($\lambda_{\text{Ex, max}} = 385 \text{ nm}$) from a Thorlabs UV-M385L2 LED was passed through a linear polarizer and irradiated on the sample through a fluorescence cube equipped with a Nikon 330-380 band-pass excitation filter, Semrock Di01-R405 dichroic mirror, and Edmund LP420 long-pass emission filter. The fluorescence spectrum was measured using a Hamamatsu PMA-12 fiber-coupled spectrometer after passing a polarizer (hereafter referred to as analyzer). The measurement spot diameter was $\sim 100 \mu\text{m}$.

2.6. Synthesis

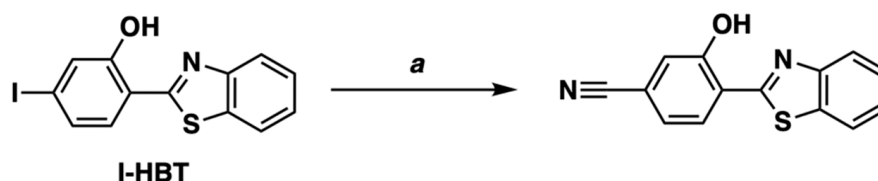
CN-HBT (2-(benzo[d]thiazol-2-yl)-5-cyanophenol). Anhydrous dimethylacetamide (DMAc) (30 mL) and one drop of poly(methylhydrosiloxane) (PMHS) was added to the mixture of **I-HBT** [11] (151 mg, 0.43 mmol), Zn(CN)₂ (52 mg, 0.45 mmol), tris(dibenzylideneacetone)dipalladium (Pd₂(dba)₃, 8.7 mg, 0.0095 mmol), and 1,1'-diphenylphosphinoferrocene (dppf, 7.4 mg, 0.013 mmol) in a 20 mL Schlenk tube under argon, and the suspension was degassed by freeze-pump-thaw cycles 3 times. The mixture was stirred at 110 °C for 23 h, and then filtered off from an insoluble fraction through silica gel by eluting with EtOAc. The filtrate was evaporated to dryness under reduced pressure, and the residue was purified by silica gel column chromatography with hexane/EtOAc (5/1 *v/v*) as an eluent to give pure **CN-HBT** in a 73% yield (0.079 g, 0.31 mmol). ¹H NMR (CDCl₃): 7.23 (dd, *J* = 8.4, 1.6 Hz, 1H, Ar-H), 7.39 (d, *J* = 1.6 Hz, 1H, Ar-H), 7.49 (td, *J* = 7.6, 0.8 Hz, 1H, Ar-H), 7.58 (td, *J* = 7.2, 1.2 Hz, 1H, Ar-H), 7.78 (d, *J* = 8.4 Hz, 1H, Ar-H), 7.96 (dd, *J* = 8.0, 1.2 Hz, 1H, Ar-H), 8.04 (d, *J* = 8.0 Hz, 1H, Ar-H), 12.86 (s, 1H, OH). ¹³C NMR (CDCl₃): 167.52, 157.98, 151.64, 132.99, 129.07, 127.40, 126.66, 122.88, 122.70, 121.90, 121.86, 120.57, 118.22, 115.44.

3. Results and Discussion

3.1. Synthesis and Characterization of CN-HBT

We turned our attention to **CN-HBT** to investigate whether the positive “triple bond” effect on the photoluminescence quantum yield is available with a cyano group in addition

to an alkynyl one. As shown in Scheme 1, the cyano group was smoothly introduced by the cross-coupling reaction of the **I-HBT** with $\text{Zn}(\text{CN})_2$ with the aid of palladium–1,1-bis(diphenylphosphino)ferrocene (dppf) complex as a catalyst [33]. The reaction mixture was easily purified and isolated by column chromatography using silica gel, and the observed peaks in ^1H and ^{13}C NMR spectra were consistently assigned (Figures 3 and S2).



Scheme 1. Synthesis of **CN-HBT**. Conditions: (a) $\text{Zn}(\text{CN})_2$, $\text{Pd}_2(\text{dba})_3$, dppf, PMHS, DMAc, 110 °C, 23 h, 73%.

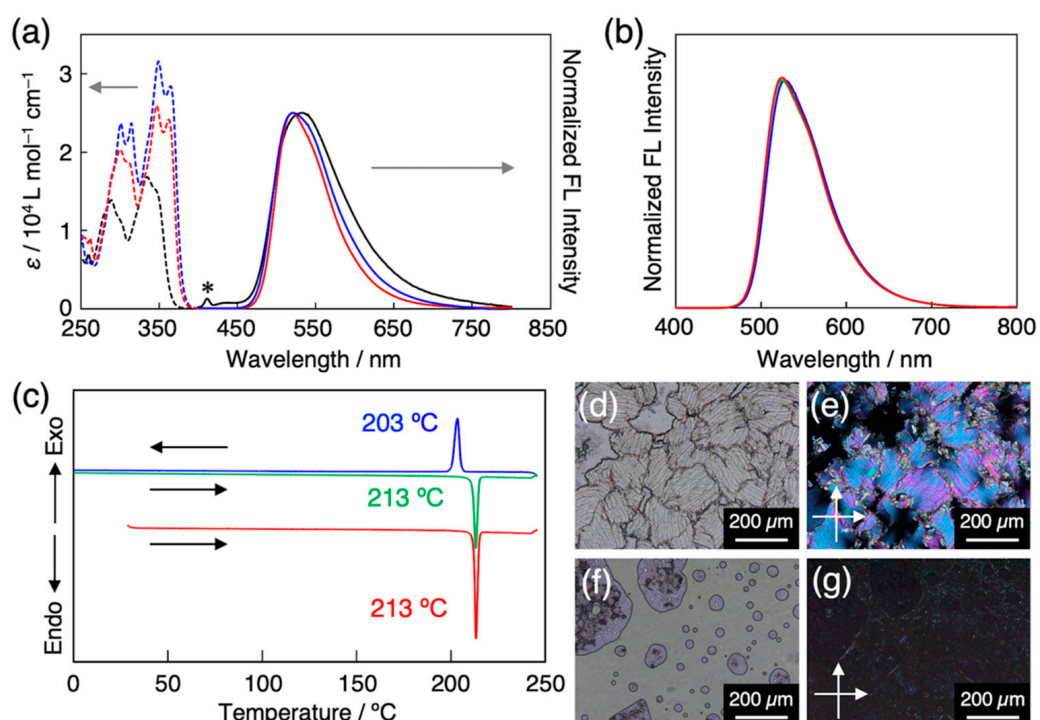


Figure 3. (a) UV-vis absorption (dashed line) and fluorescence (solid line, $\lambda_{\text{Ex}} = 365 \text{ nm}$) spectra of **HBT** (black), **C₄-C≡C-HBT** (blue), and **CN-HBT** (red) in CH_2Cl_2 ($5 \times 10^{-5} \text{ M}$). Asterisk represents Raman scattering peak from CH_2Cl_2 . (b) Fluorescence spectra ($\lambda_{\text{Ex}} = 365 \text{ nm}$) **CN-HBT** in the solid state (red), in 5CB (blue, 1/99 wt/wt), in PCH5 (green, 0.5/99.5 wt/wt). (c) DSC traces of **CN-HBT** on the 1st heating (red), 1st cooling (blue), and 2nd heating (green) at 10 K min^{-1} . Optical microscopy images of **CN-HBT** in glass cell at (d,e) 25 °C and (f,g) 220 °C (d,f) without and (e,g) with crossed polarizers.

The electronic absorption spectrum of the **CN-HBT** in CH_2Cl_2 showed peaks at 347 and 362 nm in the $\text{S}_0\text{--}\text{S}_1$ transition range, exhibiting a ca. 0.12 eV red shift from the absorption spectrum of the **HBT** (Figure 3a). The absorption edges of the **CN-HBT** and **C₄-C≡C-HBT** are almost identical to each other, which suggests that the π -conjugation degree of a cyano group is similar with that of the alkynyl group. The fluorescence spectrum of the **CN-HBT** in CH_2Cl_2 shows one broad fluorescence band with a peak at 520 nm (Figure 3a), which is assignable to the *keto** emission of HBT derivatives. No *enol** emission was observed from the **CN-HBT**, suggesting that the energy barrier of the ESIPt was small enough to undergo and the energy level of the *keto** state was much lower than that of the *enol** state. The observed large Stokes shift of 1.04 eV further supports the

ESIPT-based emission. The *keto** emission was not only observed in organic solvents but also in room-temperature nematic LCs. A small amount of **CN-HBT** was dissolved in 5CB or *trans*-4-(4-pentylcyclohexyl)benzotrile (PCH5) to yield homogeneous host–guest LCs (described later in detail). These two LCs, upon photoexcitation at 365 nm, clearly displayed fluorescence at 528 and 524 nm, respectively (Figure 3b), characterizing the ESIPT-based *keto** emission. The fact that there is no fluorescence from the 5CBs in the **CN-HBT**/5CB mixture is most probably because **CN-HBTs** are selectively excited by the 365 nm light, and a small number of directly excited 5CB molecules are quenched after transferring their energy to the **CN-HBTs**. **CN-HBT** in the solid state is photoluminescent in the same region with no significant wavelength shift (Figure 3b), implying no electronic interactions among adjacent neighboring molecules.

Differential scanning calorimetry of the **CN-HBT** powder revealed one endothermic peak at 213 °C on the 1st heating starting from 30 °C at 10 K min^{−1} (Figure 3c). It corresponds to the phase transition from crystal (Cr) to isotropic liquid (IL), which is confirmed by the disappearance of optical textures (Figure 3d) at this temperature on heating in POM with crossed polarizers. This Cr–IL transition is reproduced on the 1st cooling (203 °C), the 2nd heating (213 °C), and further heating/cooling cycles.

3.2. Preparation and Characterization of Host–Guest LCs Using **CN-HBT** as Guest Dopant

To realize light-emitting room-temperature LCs, homogeneous mixtures were prepared by mixing the **CN-HBT** in a room temperature LC as a guest luminophore. The mixtures were prepared by mixing 5CB or PCH5 with **CN-HBT** at different weight ratios in a glass vial. After checking the complete dissolution of the **CN-HBT** in the host LCs upon heating at 50 °C to form colorless transparent liquid, the liquid was cooled down to room temperature. A mixture of 5CB/**CN-HBT** (99/1 wt/wt) is visually homogeneous, but its 2 wt% (98/2 wt/wt) mixture was obviously non-homogeneous, giving small pieces of precipitated solid at room temperature. On the other hand, the PCH5/**CN-HBT** was non-homogeneous even at 1 wt% (99/1 wt/wt). A mixture containing 0.5 wt% of **CN-HBT** (99.5/0.5 wt/wt) was confirmed as a visually homogeneous mixture. The absence of alkyl chains and the presence of a cyano group may both contribute to the relatively low solubility (miscibility) compared with the HBT (maximum miscibility into 5CB: 9 wt%).

The non-homogeneity (phase separation) was also checked by means of POM and X-ray diffraction analysis. As exemplified by the 5CB/**CN-HBT** system, the 1 wt% mixture loaded in a glass cell without surface treatment showed a marble texture in POM between crossed polarizers (Figure 4a), indicating a uniform nematic LC phase at room temperature. When the mixture was heated to 40 °C, the optical textures disappeared to form an IL phase (Figure 4b). In the PCH5/**CN-HBT** (99.5/0.5 wt/wt), a typical nematic schlieren texture was observed at room temperature (Figure 4c). On the other hand, after loading the 5CB/**CN-HBT** (98/2 wt/wt) mixture into a glass cell over 40 °C and cooling it down to room temperature, needle-shaped crystals were precipitated (Figure 4d), which agrees with the precipitation behavior confirmed by the naked eye.

CN-HBT in the solid powder exhibited several diffraction peaks in the XRD (Figure 4e), which suggests that the powder is not amorphous but crystalline at room temperature. On the other hand, the 5CB/**CN-HBT** (99/1 wt/wt) gave a featureless pattern. The observed broad peak at approximately $2\theta = 20^\circ$ results from the fluctuating pentyl groups from the 5CB, which is evidenced by the XRD pattern of the 5CB alone (Figure 4e). In contrast, diffraction peaks were observed for a mixture of 5CB/**CN-HBT** (98/2 wt/wt) (Figure 4e). These peaks clearly indicate the formation of **CN-HBT** crystallites in the mixture, since the pattern and peak positions of the **CN-HBT** and 5CB/**CN-HBT** (98/2 wt/wt) resemble one another. The homogenous mixtures were further characterized by DSC. The peaks observed during the 1st cooling and 2nd heating, observed in the 5CB/**CN-HBT** (99/1 and 98/2 wt/wt), denote a phase transition between nematic LC and the IL phase (Figure 4f). The single transition of N–IL phases in the 5CB/**CN-HBT** (98/2 wt/wt) is against our initial expectation because the mixture is non-homogeneous

judging from the POM and XRD measurements. However, we considered that the mixture became a homogeneous nematic LC state between 25 and 34 °C due to the increased solubility upon elevating the temperature, and thus showed a single N–IL transition in the DSC. Overall, based on the visual and POM observations, as well as XRD analysis, we concluded that the **CN-HBT** is miscible and serves as a fluorescent dopant in the 5CB and PCH5 up to 1wt% (=1 mol%) and 0.5 wt% (=0.5 mol%), respectively.

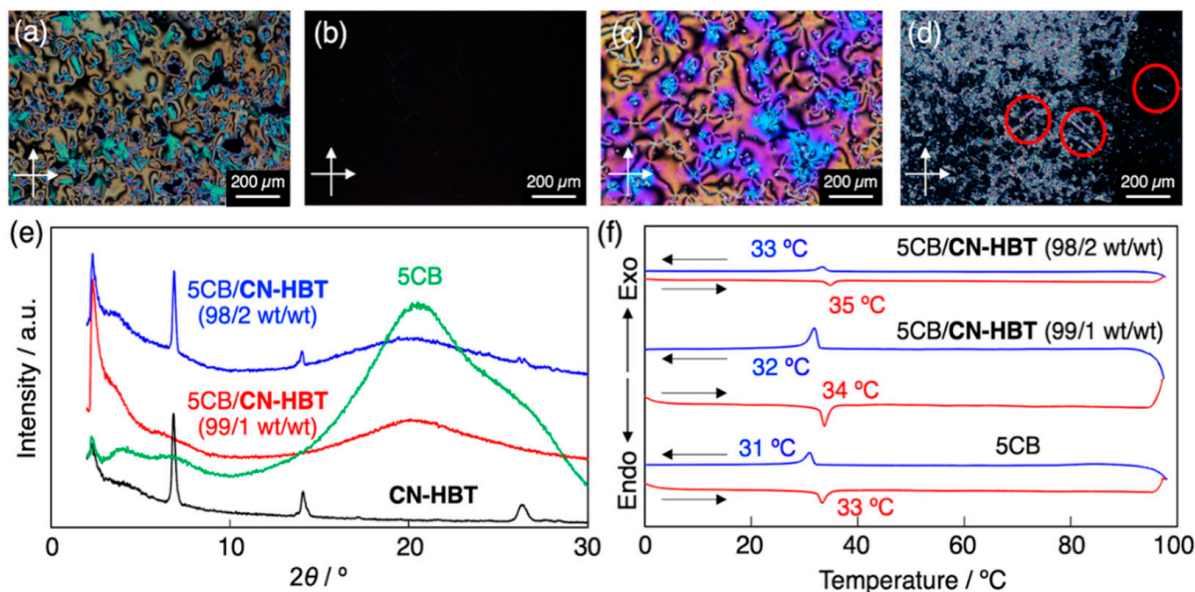


Figure 4. Cross-polarized optical microscopy images of (a,b) 5CB/CN-HBT (99/1 wt/wt) at (a) 25 °C and (b) 40 °C, (c) PCH5/CN-HBT (0.5/99.5 wt/wt) at 25 °C, and (d) 5CB/CN-HBT (98/2 wt/wt) at 25 °C in a glass sandwiched cell. Red circles represent needle-shaped microcrystals. (e) XRD patterns of **CN-HBT** (black), 5CB (green), 5CB/CN-HBT (99/1 wt/wt) (red), and 5CB/CN-HBT (98/2 wt/wt) (blue). The incident X-ray wavelength was $\lambda = 1.54 \text{ \AA}$. (f) DSC traces of 5CB and 5CB/CN-HBT (99/1 and 98/2, wt/wt) on 1st cooling (blue), and 2nd heating (red) at 10 K min^{-1} .

3.3. Rate Constant Analysis of Photoluminescence of CN-HBT in Solution and Nematic LCs

We discuss the impact of a cyano group on the photoluminescence behavior of the HBT motif from the aspect of radiative (fluorescence) and nonradiative rate constants, k_r and k_{nr} , respectively. When the fluorescence decay follows a single exponential equation, the values of k_r and k_{nr} can be estimated by the following well-known equations,

$$\Phi_{FL} = k_r (k_r + k_{nr})^{-1} \quad (1)$$

$$\tau_{FL} = (k_r + k_{nr})^{-1} \quad (2)$$

where Φ_{FL} and τ_{FL} denote an absolute fluorescence quantum yield and fluorescence lifetime, respectively. These parameters were evaluated by fluorescence spectroscopy using an integrated sphere and transient fluorescence spectroscopy with photoexcitation at 365 nm. The obtained values for both in the CH_2Cl_2 and 5CB are summarized in Table 1. The most interesting finding here is the remarkably large Φ_{FL} value of 0.49 for **CN-HBT** in CH_2Cl_2 , which is much larger than that of the previously-reported hexynyl analogue ($\text{C}_4\text{-C}\equiv\text{C-HBT}$, $\Phi_{FL} = 0.07$). In 5CB, **CN-HBT** marked $\Phi_{FL} = 0.57$ that is still significantly larger than that of $\text{C}_4\text{-C}\equiv\text{C-HBT}$ ($\Phi_{FL} = 0.32$). The values of τ_{FL} reveal a good correlation with the substituents—the order of the lifetime length is **CN-HBT** > $\text{C}_4\text{-C}\equiv\text{C-HBT}$ > HBT. As shown in Table 1, the values of k_r are almost constant at $\sim 1 \times 10^8 \text{ s}^{-1}$, while k_{nr} ranges from $\sim 10^0 \times 10^8$ to $\sim 10^2 \times 10^8 \text{ s}^{-1}$. The former indicates the negligible impact of both the local dipoles and extended conjugations on total transition dipole moments from all orbitals. The nonradiative decay processes are restricted by the introduction of the alkynyl groups [12], but we discovered that the cyano group has a much

greater effect. Considering that the fluorescence is emitted from single molecules in diluted solutions and LC matrices, the nonradiative decays likely originate from a structural relaxation around carbon–carbon bond rotation between 2-hydroxyphenyl and benzothiazole units. Our experimental observations suggest that a remote manipulation to suppress the nonradiative decays is certainly possible, without changing the fluorescence energy (wavelength), by incorporating appropriate substituents on the 2-hydroxyphenyl part. The energy landscape at the excited states is currently under investigation and is expected to provide an explanation for the unexpectedly high efficiency induced by the cyano group in suppressing the nonradiative decay processes from S_1 to S_0 [12,14,34].

Table 1. Fluorescent quantum yield Φ_{FL} , fluorescence lifetime τ_{FL} , and radiative rate constant k_r and nonradiative rate constant k_{nr} for HBT, $C_4-C\equiv C-HBT$, and $CN-HBT$ in CH_2Cl_2 (5×10^{-5} M) and 5CB (1/99 wt/wt) ($\lambda_{Ex} = 365$ nm).

	$\Phi_{FL}/-$		τ_{FL}/ns		$k_r/10^8 s^{-1}$		$k_{nr}/10^8 s^{-1}$	
	in CH_2Cl_2	in 5CB	in CH_2Cl_2	in 5CB	in CH_2Cl_2	in 5CB	in CH_2Cl_2	in 5CB
HBT	0.01	0.07	0.10	0.98	1.0	0.72	102	9.5
$C_4-C\equiv C-HBT$	0.07 ¹	0.32 ¹	0.85	2.95	0.8	1.1	11	2.3
CN-HBT	0.49	0.57	4.81	4.94	1.0	1.1	1.1	0.87

¹ Ref. [12].

3.4. Polarizing Absorption and Fluorescence Spectra

The alignment of the luminescent molecules plays an important role in obtaining polarized fluorescence with a high dichroic ratio [35–37]. Taking advantage of the potential of **CN-HBT** as a colorless fluorescent dopant with a high Φ_{FL} of 0.57, basic properties including polarized absorption and photoluminescence were evaluated for the host–guest LC composed of 5CB and **CN-HBT**. The 5CB/**CN-HBT** (99/1 wt/wt) mixture was loaded, by capillary action, into a 15 μ m gap sandwiched ITO-glass cell whose surfaces are coated with an antiparallel-rubbed polyimide. This surface treatment induces the uniaxial alignment of the long molecular axis of the 5CB in the nematic phase. Surrounded by the aligned 5CB molecules, the dispersed dopant molecules **CN-HBTs** are forced to align roughly in the same direction, even though the shape of the **CN-HBT** molecules themselves is not a typical rod.

Figure 5 represents the polarized absorption spectra measured with a polarizer inserted into the optical path. The LC cell filled with 5CB absorbed light due to the presence of ITO, glass, polyimide surface, and 5CB. The difference of absorbance depending on the polarizer directions (parallel // or perpendicular \perp) appeared below ~ 345 nm, indicating the absorption by 5CB takes place in this region. The absorption over ~ 345 nm should derive from ITO and pseudo-absorption due to the light scattering. Then, the cell filled with 5CB/**CN-HBT** (99/1 wt/wt) afforded absorption spectra with characteristic two peaks over 345 nm that originates from aligned **CN-HBT** molecules. The polarized light in the parallel direction was more absorbed than that in the perpendicular direction. The dichroic ratio was calculated as $D_A = 2.9$, according to the equation of $\Delta A_{//,367nm} / \Delta A_{\perp,367nm}$, where the definition of each absorbance is indicated in Figure 5. Similarly, the degree of polarization, ρ_A , was calculated as 0.48 by Equation (3) [38],

$$\rho_A = (A_{//} - A_{\perp}) / (A_{//} + A_{\perp}) \quad (3)$$

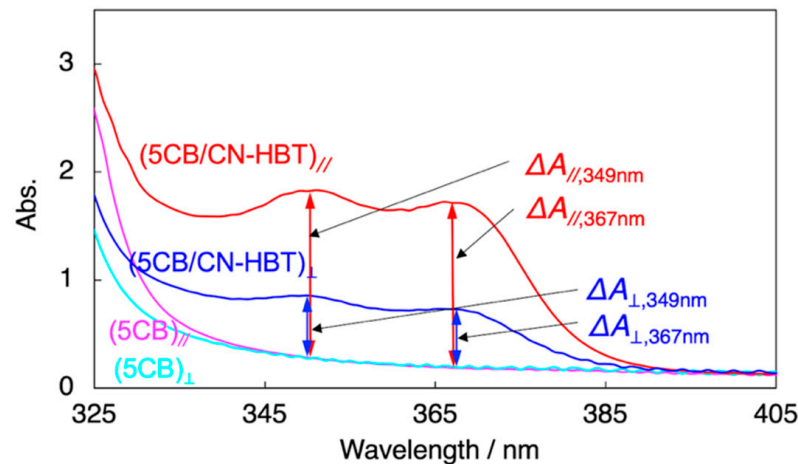


Figure 5. Polarized absorption spectra of 5CB (turquoise, magenta) and 5CB/CN-HBT (99/1 wt/wt) (red, blue) in 15- μm thick LC cell. The surface of two ITO-glass substrates consisting of the LC cell is coated with rubbed polyimides with a parallel direction. The incident light was polarized at 0° (magenta, red) and 90° (turquoise, blue) from the orientational axis of the cell.

Supposing that the dihedral angle between the long molecular axis and transition dipole is small (roughly estimated as $\sim 5^\circ$), the order parameter S_A was evaluated as 0.38 according to the Equation (4) [38],

$$S_A = (A_{//} - A_{\perp}) / (A_{//} + 2A_{\perp}) \quad (4)$$

Although these anisotropic parameters are all smaller than the previous HBT-based dopants developed by our group [11,12,14], it is worth noting that CN-HBT, without alkyl chains, can align parallel to the direction of 5CB and exhibits an anisotropic absorption capability.

Polarizing fluorescence microscopy was carried out to measure the anisotropic fluorescence of the CN-HBT molecules uniaxially aligned in the 5CB host (Figure 6a). Figure 6b shows the dependence of the fluorescence spectrum on the analyzer angle. As expected, the fluorescence intensity is highest when the analyzer is parallel ($=0^\circ$) to the alignment direction (=director \mathbf{n}) and lowest when the analyzer is perpendicular ($=90^\circ$). The dichroic ratio is calculated in a similar manner to the absorbance as $D_{FL} = I_{//} / I_{\perp}$, where $I_{//}$ and I_{\perp} are the fluorescence intensities at the analyzer angles of 0° and 90° , respectively. The calculated value of D_F is 3.1 at $\lambda_{Em} = 528 \text{ nm}$ (Figure 6c), which is similar to the absorption anisotropy. The degree of polarization (ρ_F) and order parameter (S_F) were also evaluated in the same way as polarizing absorption spectroscopy according to Equations (5) and (6),

$$\rho_F = (I_{//} - I_{\perp}) / (I_{//} + I_{\perp}) \quad (5)$$

$$S_F = (I_{//} - I_{\perp}) / (I_{//} + I_{\perp}) \quad (6)$$

The calculated values of ρ_{FL} and S_{FL} are 0.51 and 0.41, respectively. These values are slightly smaller than those of C₄-C≡C-HBT, which may be due to the absence of a terminal alkyl chain which is compatible with 5CB molecules.

Electric field-induced reorientation was confirmed by applying a square wave voltage with a frequency of 1 kHz between the ITO-glass substrates of the cell. Under an applied field, the LC reorients to align its direction parallel to the electric field owing to the positive dielectric anisotropy. Because the transition dipole moment of the CN-HBT also realigns with the field, the polarization properties vary respectively. Figure 6d shows the voltage dependence of the fluorescence spectrum measured with the excitation light polarization and analyzer transmission axis both directed along the rubbing axis. Above approximately 2 V, the fluorescence intensity saturates at approximately 25% of the initial intensity. In this

regime, the analyzer angle dependence becomes almost unnoticeable (Figure 6e), because most of the molecules are aligned vertically to the substrates, and the detected fluorescence only contains components emitted perpendicular to the transition dipole moment. The polarized fluorescence properties and electric field response reveal the potential of the field-responsive, light-emitting host–guest room-temperature LC systems utilizing CN-HBT as a highly efficient fluorescent dopant.

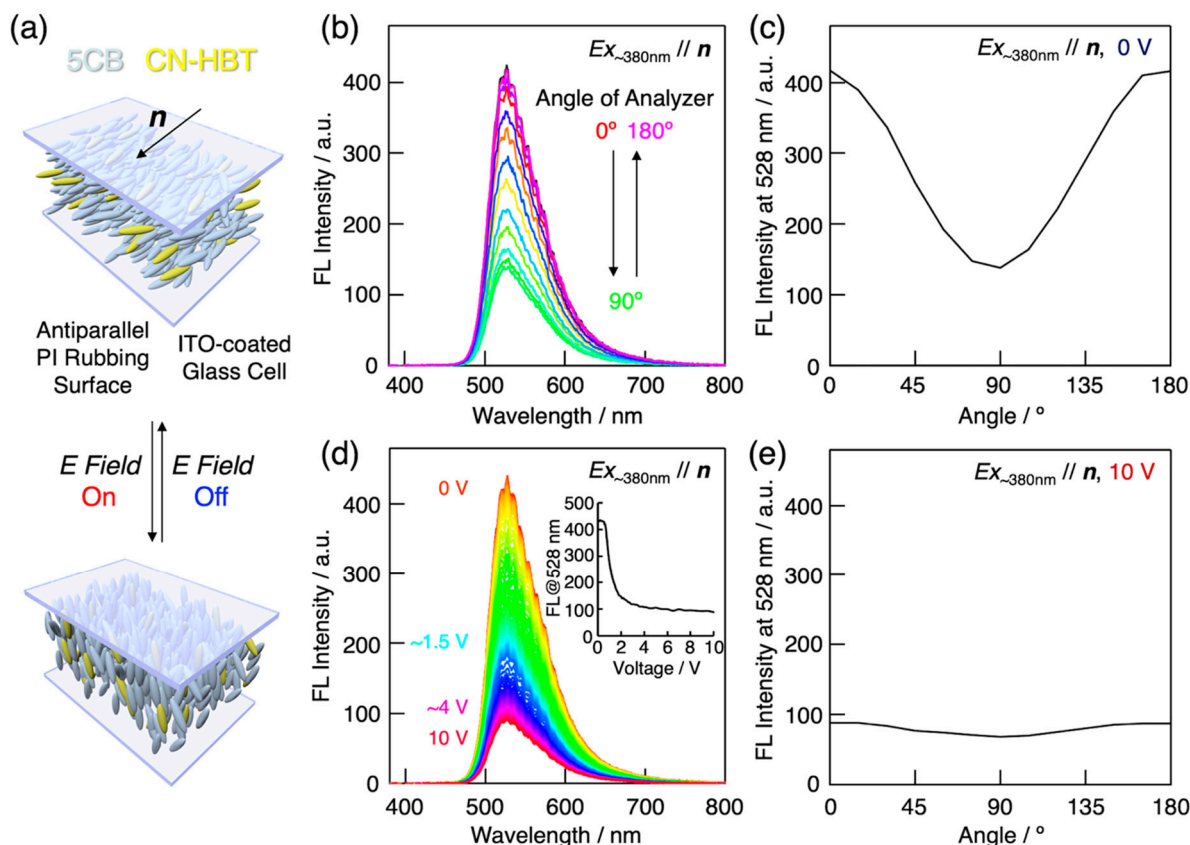


Figure 6. (a) Schematic illustrations of 5CB/CN-HBT host–guest LCs in sandwiched ITO-glass cell with surface polyimide (PI) rubbing in antiparallel directions. Gray- and yellow-colored rod-shaped objects represent 5CB and CN-HBT molecules, respectively. The LC director (n) orients along the rubbing axis at zero field and reorients to become perpendicular to the substrates when the electric field is applied. (b) Analyzer angle dependence of the fluorescence spectrum of 5CB/CN-HBT (99/1 wt/wt) in a 15- μm thick antiparallel PI rubbing LC cell. The excitation light ($\lambda_{\text{Ex}} = 385 \text{ nm}$) is polarized parallel to the rubbing axis (i.e., n) and the analyzer angle is measured from the rubbing axis. (c) Polarization dependence of fluorescence intensity at 528 nm in (a). (d) Applied voltage dependence of the fluorescence spectrum of 5CB/CN-HBT (99/1 wt/wt). Inset represents fluorescence intensity at 528 nm as function of applied voltage. (e) Polarization dependence of fluorescence intensity at 528 nm and applied voltage of 10 V.

4. Conclusions

The photoluminescent properties of an ESIPT luminophore, 2-(2-hydroxy-4-cyanophenyl)benzothiazole (2-(benzo[*d*]thiazol-2-yl)-5-cyanophenol), were newly studied in detail. This cyano-substituted HBT, named CN-HBT, only showed *keto** emission in CH_2Cl_2 , LCs (5CB and PCH5), and in the powder state, suggesting that the energy barrier of the ESIPT was small enough to undergo and the energy level of the *keto** state was much lower than that of the *enol** state. CN-HBT marked a fluorescence quantum yield (Φ_{FL}) of 0.49 in CH_2Cl_2 that is much larger than HBT ($\Phi_{\text{FL}} = 0.01$) and 1-hexynyl-substituted HBT ($\Phi_{\text{FL}} = 0.07$), characterizing the prominent effect of cyano substitution. Its high fluorescent quantum yield is also retained in nematic LCs ($\Phi_{\text{FL}} = 0.57$ in 5CB) and it can be homogeneously miscible in 5CB up to 1 wt%. Based on the experimental analysis of radiative (k_r)/nonradiative (k_{nr}) rate constants for the HBT series, it became clear that CN-

HBT suppresses nonradiative decays while keeping the almost constant k_r . Surprisingly, the value of k_{nr} for the **CN-HBT** is 1% and 10% of that for HBT in CH_2Cl_2 and 5CB, respectively. A host–guest light-emitting LC, prepared by the combination of 5CB and **CN-HBT** with 99/1 wt/wt blend ratio, is able to uniaxially align in LC cells and showed anisotropic absorption in the range of electronic transition of the **CN-HBT**. Upon polarized UV excitation, the **CN-HBT**-doped LC emits anisotropic fluorescence with a dichroic ratio of ~ 3.1 . The out-of-plane fluorescence intensity can also be controlled by applying an electric field that causes the molecules to align perpendicular to the substrate plane. The doping method demonstrated in the present work conveniently provides light-emitting LCs with tunable anisotropic luminescence controllable by macroscopic orientations. Especially, we disclosed that the introduction of a cyano group into HBT is a promising approach for yielding a fluorescence dopant molecule that is transparent in the visible region and emits a green light efficiently upon photoexcitation by UV light. Further exploration of the molecular designing on ESIPT fluorophores stands a chance of developing efficient, highly-miscible, and color-tunable fluorescent dopants useful for host-guest LCs.

Supplementary Materials: The following are available online at <https://www.mdpi.com/article/10.3390/cryst11091105/s1>, Figure S1: Summary of molecular structures, abbreviated names, and fluorescence quantum yields of HBT derivatives reported in previous and this works, Figure S2: ^1H NMR spectrum of **CN-HBT**, Figure S3: ^{13}C NMR spectrum of **CN-HBT**.

Author Contributions: Design of project, T.S.; Synthesis of **CN-HBT**, M.K.; UV and FL measurements, M.K. and T.S.; DSC, POM, and XRD measurements, M.K. and T.S.; Fluorescence lifetime measurement, M.K., T.S. and M.S.; Polarized absorption measurements, M.K. and T.S.; Polarized fluorescence measurements, H.Y.; Writing a draft, T.S., M.K., H.Y. and M.S. All authors have read and agreed to the published version of the manuscript.

Funding: This work was partly supported by a Grant-in-Aid for Scientific Research (No. 20H02710 and 19H02581) and for Challenging Research (Exploratory) (No. 20K21154) from the Japan Society for the Promotion of Science (JSPS), and a research grant from the Futaba Foundation. This work was partly supported by using research equipment shared in MEXT project for promoting public utilization of advanced research infrastructure (Program for supporting introduction of the new sharing system, No. JPMXS0421800120).

Institutional Review Board Statement: Not applicable.

Informed Consent Statement: Not applicable.

Acknowledgments: T.S. and H.Y. thanks the Leading Initiative for Excellent Young Researchers program by Ministry of Education, Culture, Sports, Science and Technology (MEXT), Japan.

Conflicts of Interest: The authors declare no conflict of interest.

References

1. Raj, D. Dichroic display technology potentials and limitations. *Mater. Chem. Phys.* **1996**, *43*, 204–211. [[CrossRef](#)]
2. Weder, C.; Sarwa, C.; Montali, A.; Bastiaansen, C.; Smith, P. Incorporation of photoluminescent polarizers into liquid crystal displays. *Science* **1998**, *279*, 835–837. [[CrossRef](#)]
3. Wang, Y.; Shi, J.; Chen, J.; Zhu, W.; Baranoff, E. Recent progress in luminescent liquid crystal materials: Design, properties and application for linearly polarised emission. *J. Mater. Chem. C* **2015**, *3*, 7993–8005. [[CrossRef](#)]
4. Zhao, D.; Bi, W.; Tang, B.Z. A light-emitting liquid crystal display device without polarizers and alignment layers. *Adv. Opt. Mater.* **2021**, *9*, 2100489. [[CrossRef](#)]
5. Heilmeier, G.H.; Zaroni, L.A. Guest-host interactions in nematic liquid crystals. A new electro-optic effect. *Appl. Phys. Lett.* **1968**, *13*, 91–92. [[CrossRef](#)]
6. White, D.L.; Taylor, G.N. New absorptive mode reflective liquid-crystal display device. *J. Appl. Phys.* **1974**, *45*, 4718–4723. [[CrossRef](#)]
7. Sims, M.T. Dyes as guests in ordered systems: Current understanding and future directions. *Liq. Cryst.* **2016**, *43*, 2363–2374. [[CrossRef](#)]
8. Lutfor, M.R.; Hegde, G.; Kumar, S.; Tschierske, C.; Chigrinov, V.G. Synthesis and characterization of bent-shaped azobenzene monomers: Guest-host effects in liquid crystals with Azo dyes for optical image storage devices. *Opt. Mater.* **2009**, *32*, 176–183. [[CrossRef](#)]

9. Carrasco-Vela, C.; Quintana, X.; Oton, E.; Geday, M.; Otón, J. Security devices based on liquid crystals doped with a colour dye. *Opto-Electron. Rev.* **2011**, *19*, 496–500. [[CrossRef](#)]
10. Kim, M.; Park, K.J.; Seok, S.; Ok, J.M.; Jung, H.-T.; Choe, J.; Oh, D.H.; Kim, D.H. Fabrication of microcapsules for dye-doped polymer-dispersed liquid crystal-based smart windows. *ACS Appl. Mater. Interfaces* **2015**, *7*, 17904–17909. [[CrossRef](#)]
11. Zhang, W.; Sakurai, T.; Aotani, M.; Watanabe, G.; Yoshida, H.; Padalkar, V.S.; Tsutsui, Y.; Sakamaki, D.; Ozaki, M.; Seki, S. Highly fluorescent liquid crystals from excited-state intramolecular proton transfer molecules. *Adv. Opt. Mater.* **2019**, *7*, 1801349. [[CrossRef](#)]
12. Zhang, W.; Suzuki, S.; Cho, S.; Watanabe, G.; Yoshida, H.; Sakurai, T.; Aotani, M.; Tsutsui, Y.; Ozaki, M.; Seki, S. Highly miscible hybrid liquid-crystal systems containing fluorescent excited-state intramolecular proton transfer molecules. *Langmuir* **2019**, *35*, 14031–14041. [[CrossRef](#)]
13. Tsutsui, Y.; Zhang, W.; Ghosh, S.; Sakurai, T.; Yoshida, H.; Ozaki, M.; Akutagawa, T.; Seki, S. Electrically switchable amplified spontaneous emission from liquid crystalline phase of an AIEE-active ESIPT molecule. *Adv. Opt. Mater.* **2020**, *8*, 1902158. [[CrossRef](#)]
14. Zhang, W.; Suzuki, S.; Sakurai, T.; Yoshida, H.; Tsutsui, Y.; Ozaki, M.; Seki, S. Extended conjugation of ESIPT-type dopants in nematic liquid crystalline phase for enhancing fluorescence efficiency and anisotropy. *Phys. Chem. Chem. Phys.* **2020**, *22*, 28393–28400. [[CrossRef](#)] [[PubMed](#)]
15. Barbara, P.F.; Brus, L.E.; Rentzepis, P.M. Intramolecular proton transfer and excited-state relaxation in 2-(2-hydroxyphenyl)benzothiazole. *J. Am. Chem. Soc.* **1980**, *102*, 5631–5635. [[CrossRef](#)]
16. Potter, C.A.S.; Brown, R.G.; Vollmer, F.; Rettig, W. Role of twisted intramolecular charge-transfer states in the decay of 2-(2'-hydroxyphenyl)benzothiazole following excited-state intramolecular proton transfer. *J. Chem. Soc. Faraday Trans.* **1994**, *90*, 59–67. [[CrossRef](#)]
17. Barbatti, M.; Aquino, A.J.A.; Lischka, H.; Schrieffer, C.; Lochbrunner, S.; Riedle, E. Ultrafast internal conversion pathway and mechanism in 2-(2'-hydroxyphenyl)benzothiazole: A case study for excited-state intramolecular proton transfer systems. *Phys. Chem. Chem. Phys.* **2009**, *11*, 1406–1415. [[CrossRef](#)]
18. Pigeau, S.; Foster, D.; Hohenstein, E.G. Excited-state dynamics of 2-(2'-Hydroxyphenyl)benzothiazole: Ultrafast proton transfer and internal conversion. *J. Phys. Chem. A* **2017**, *121*, 4595–4605. [[CrossRef](#)]
19. Mei, J.; Leung, N.L.C.; Kwok, R.T.K.; Lam, J.W.Y.; Tang, B.Z. Aggregation-induced emission: Together we shine, united we soar! *Chem. Rev.* **2015**, *115*, 11718–11940. [[CrossRef](#)]
20. Crespo-Otero, R.; Li, Q.; Blancafort, L. Exploring potential energy surfaces for aggregation-induced emission—From solution to crystal. *Chem. Asian J.* **2018**, *14*, 700–714. [[CrossRef](#)]
21. Haidekker, M.A.; Theodorakis, E.A. Environment-sensitive behavior of fluorescent molecular rotors. *J. Biol. Eng.* **2010**, *4*, 11. [[CrossRef](#)] [[PubMed](#)]
22. Vyšniauskas, A.; Kuimova, M.K. A twisted tale: Measuring viscosity and temperature of microenvironments using molecular rotors. *Int. Rev. Phys. Chem.* **2018**, *37*, 259–285. [[CrossRef](#)]
23. Massue, J.; Ulrich, G.; Ziessel, R. Effect of 3,5-disubstitution on the optical properties of luminescent 2-(2-Hydroxyphenyl)benzoxazoles and their borate complexes. *Eur. J. Org. Chem.* **2013**, *2013*, 5701–5709. [[CrossRef](#)]
24. Houari, Y.; Charaf-Eddin, A.; Laurent, A.D.; Massue, J.; Ziessel, R.; Ulrich, G.; Jacquemin, D. Modeling optical signatures and excited-state reactivities of substituted hydroxyphenylbenzoxazole (HBO) ESIPT dyes. *Phys. Chem. Chem. Phys.* **2014**, *16*, 1319–1321. [[CrossRef](#)] [[PubMed](#)]
25. Massue, J.; Jacquemin, D.; Ulrich, G. Molecular engineering of excited-state intramolecular proton transfer (ESIPT) dual and triple emitters. *Chem. Lett.* **2018**, *47*, 1083–1089. [[CrossRef](#)]
26. Munch, M.; Curtil, M.; Vérité, P.M.; Jacquemin, D.; Massue, J.; Ulrich, G. Ethynyl-tolyl extended 2-(2'-Hydroxyphenyl)benzoxazole dyes: Solution and solid-state excited-state intramolecular proton transfer (ESIPT) emitters. *Eur. J. Org. Chem.* **2019**, *2019*, 1134–1144. [[CrossRef](#)]
27. Pariat, T.; Munch, M.; Durko-Maciąg, M.; Mysliwiec, J.; Retailleau, P.; Vérité, P.M.; Jacquemin, D.; Massue, J.; Ulrich, G. Impact of heteroatom substitution on dual-state emissive rigidified 2-(2'-hydroxyphenyl)benzazole dyes: Towards ultra-bright ESIPT fluorophores. *Chem. Eur. J.* **2021**, *27*, 3483–3495. [[CrossRef](#)]
28. Wang, Q.; Xu, L.; Niu, Y.; Wang, Y.; Yuan, M.-S.; Zhang, Y. Excited state intramolecular proton transfer in ethynyl-extended regioisomers of 2-(2'-Hydroxyphenyl)benzothiazole: Effects of the position and electronic nature of substituent groups. *Chem. Asian J.* **2016**, *11*, 3454–3464. [[CrossRef](#)]
29. Xu, L.; Wang, Q.; Zhang, Y. Electronic effect on the photophysical properties of 2-(2-hydroxyphenyl)benzothiazole-based excited state intramolecular proton transfer fluorophores synthesized by sonogashira-coupling reaction. *Dye. Pigment.* **2017**, *136*, 732–741. [[CrossRef](#)]
30. Shah, S.S.; Paul, A.; Bera, M.; Venkatesh, Y.; Singh, N.D.P. Metallaphotoredox-Mediated C_{sp2}-H Hydroxylation of Arenes under Aerobic Conditions. *Org. Lett.* **2018**, *20*, 5533–5536. [[CrossRef](#)]
31. Shah, S.S.; Shee, M.; Singh, A.K.; Paul, A.; Singh, N.D.P. Direct oxygenation of CH bonds through photoredox and palladium catalysis. *J. Org. Chem.* **2020**, *85*, 3426–3439. [[CrossRef](#)]
32. Bross, A.D.; Pla-Dalmau, A.; Spangler, C.W. Radiation damage to 2-(2'-Hydroxyphenyl)benzothiazoles. *Radiat. Phys. Chem.* **1993**, *41*, 379–387. [[CrossRef](#)]

33. Iqbal, Z.; Lyubimtsev, A.; Hanack, M. Synthesis of phthalonitriles using a palladium catalyst. *Synlett* **2008**, *19*, 2287–2290.
34. Suzuki, S.; Sasaki, S.; Sairi, A.S.; Iwai, R.; Tang, B.Z.; Konishi, G.-I. Principles of aggregation-induced emission: Design of deactivation pathways for advanced AIEgens and applications. *Angew. Chem. Int. Ed.* **2020**, *59*, 9856–9867. [[CrossRef](#)]
35. Gim, M.-J.; Turlapati, S.; Debnath, S.; Rao, N.V.S.; Yoon, D.K. Highly polarized fluorescent illumination using liquid crystal phase. *ACS Appl. Mater. Interfaces* **2016**, *8*, 3143–3149. [[CrossRef](#)] [[PubMed](#)]
36. Sha, J.; Lu, H.; Zhou, M.; Xia, G.; Fang, Y.; Zhang, G.; Qiu, L.; Yang, J.; Ding, Y. Highly polarized luminescence from an AIEE-active luminescent liquid crystalline film. *Org. Electron.* **2017**, *50*, 177–183. [[CrossRef](#)]
37. Lu, H.; Xu, C.; Li, Z.; Xia, G.; Jing, S.; Bai, X.; Yang, J.; Qiu, L.; Ding, Y. High-contrast electrically switchable light-emitting liquid crystal displays. *Liq. Cryst.* **2018**, *45*, 32–39. [[CrossRef](#)]
38. Ranjkesh, A.; Choi, J.-C.; Joo, K.-I.; Park, H.-W.; Zakerhamidi, M.S.; Kim, H.-R. Linear Dichroism and order parameters of nematics doped with azo dyes. *Mol. Cryst. Liq. Cryst.* **2017**, *647*, 107–118. [[CrossRef](#)]